



Internal and forced ocean variability in the Mediterranean Sea

Roberta Benincasa¹, Giovanni Liguori^{2,3}, Nadia Pinardi^{1,3}, and Hans von Storch⁴

¹Department of Physics and Astronomy, University of Bologna, Bologna, Italy

²Department of Biological, Geological, and Environmental Sciences, University of Bologna, Bologna, Italy

³Centro Euro-Mediterraneo sui Cambiamenti Climatici, Lecce, Italy

⁴Helmholtz-Zentrum Hereon, Institute for Coastal Systems, Geesthacht, Germany

Correspondence: Roberta Benincasa (roberta.benincasa2@unibo.it)

Received: 19 December 2023 – Discussion started: 3 January 2024

Revised: 12 May 2024 – Accepted: 26 June 2024 – Published: 15 August 2024

Abstract. Two types of variability are discernible in the ocean: a response to the atmospheric forcing and the so-called internal/intrinsic ocean variability, which is associated with internal instabilities, nonlinearities, and the interactions between processes at different scales. Producing an ensemble of 20 multiyear ocean simulations of the Mediterranean Sea, initialized with different realistic initial conditions but using the same atmospheric forcing, the study examines the intrinsic variability in terms of its spatial distribution and seasonality. In general, the importance of the external forcing decreases with depth but dominates in extended shelves such as the Adriatic Sea and the Gulf of Gabes. In the case of temperature, the atmospheric forcing plays a major role in the uppermost 50 m of the water column during summer and the uppermost 100 m during winter. Additionally, intrinsic variability displays a distinct seasonal cycle in the surface layers, with a prominent maximum at around 30 m depth during the summer connected to the summer thermocline formation processes. Concerning current velocity, the internal variability has a significant influence at all depths.

duration for which accurate predictions can be made and hinder the practical applications that rely on these forecast products.

Lorenz (1975) identified two types of uncertainties affecting predictability in the climate system: the predictability of the first kind derives from the resolution of an initial value problem, i.e., predicting future states of the system given the same external forcing and different initial conditions, whereas the predictability of the second kind is connected to the boundary value problem and deals with the response of the system to changes in the external forcings. In the uncoupled ocean prediction problem, the predictability of the second kind is connected to the atmospheric fluxes at the air–sea interface, while the predictability of the first kind is connected to the mesoscale and submesoscale flow field that in turn is generated by mean flow instabilities and eddy–mean flow interaction processes (Soldatenko and Yusupov, 2017).

The understanding of how internal variability can affect climate predictability and justify the observed red profile of the climate variance spectra was first achieved by Hasselmann (1976). To demonstrate the importance of internal variability in climate models, Hasselmann formulated a stochastic climate model whose main assumption is that the climate system may be divided into rapidly varying, random components and a slowly responding part. Climate variability is then shown to be due to the internal random components. The slow component behaves as an integrator of these inputs, whereas the fast component supplies the slow component with energy, allowing the existence of internal variability in the climate system. Moreover, Hasselmann proved that climate variability would grow indefinitely without a stabilizing internal feedback mechanism. Consequently, the investi-

1 Introduction

High-resolution numerical ocean models are currently employed in operational ocean forecasting, providing short-term forecasts with a lead time of 14 d for both global and regional seas, as described by Le Traon et al. (2019) and Copini et al. (2023). Consequently, comprehending the uncertainties associated with these forecasts is crucial for enhancing future ocean forecasting. Model uncertainties restrict the

gation of climate variability must be shifted from looking for positive to negative feedbacks that allow the climate system to reach stationarity in the absence of any external forcing. In the same years as Hasselmann's study, mesoscale eddies and flow instabilities were mapped for the first time in the ocean (Harrison and Robinson, 1978; McWilliams, 1996), and the presence of intense ocean internal variability was verified to exist.

The *internal variability*, or equivalently *intrinsic* or *stochastic* variability, is ubiquitous in the climate system, and it is due to both the nonlinearity and the numerous degrees of freedom of climate itself (von Storch et al., 2001). Understanding the internal variability enables us to statistically determine if a change is consistent with internal variability or instead at least partly related to external factors. Investigations into internal ocean variability with an ensemble approach were first found in the literature starting in the 2000s when eddy-resolving global ocean models were introduced (Jochum and Murtugudde, 2004, 2005; Arbic et al., 2014; Sérazin et al., 2015; Bessières et al., 2017; Leroux et al., 2018). The first extensive study on the role of internal variability in the global ocean was done by Penduff et al. (2018). They showed that mesoscales compose the ocean stochastic elements of the climate system and highlighted the necessity to adopt ensemble methods. Moreover, they showed that in several areas the internal ocean variability is more significant than atmospheric variability as a contribution to climate variability for both “the low-frequency variability and the long-term trends of regional ocean heat content” (Penduff et al., 2018). Similarly, in the study by Hogan and Sriver (2019) it was shown that internal variability is fundamental in setting the timescale for the ocean temperature adjustment process, increasing the speed at which the ocean takes up heat from the atmosphere, which is instead highly underestimated by just considering atmospheric variability. Lastly, as regards the scale dependency of the internal variability, it was demonstrated by Tang et al. (2019) that additional intrinsic variability is produced by increasing the horizontal spatial resolution of ocean models from 1 to 0.04°. Furthermore, Tang et al. (2020) analyzed the ratio of the externally forced response and the internally generated variability in the South China Sea and showed that the external forcing is dominant at large scales, while most of the variability is internally generated at smaller scales.

Our paper addresses the predictability of the first kind for the Mediterranean Sea, focusing on the internal variability, following the methodology of Penduff et al. (2018), Leroux et al. (2018), Tang et al. (2020), and Lin et al. (2022).

The Mediterranean Sea is a semi-enclosed basin with an average depth of 1500 m, and it is connected to the Atlantic Ocean through the Strait of Gibraltar and to the Marmara Sea through the Dardanelles. The external forcings are the wind stress, responsible for the permanent gyres of the basin (Pinardi et al., 2015), and the heat and water fluxes that control the overturning circulation (Pinardi et al., 2019).

Furthermore, ocean circulation in the Mediterranean Sea is characterized by significant interactions between different scales (Robinson et al., 2001), and mesoscale variability is intense, producing 50 %–60 % of ocean kinetic energy variability (Bonaduce et al., 2021). Mesoscales, for example, are associated with instabilities of the main flow, and they have a role in water mass transport across the basin (Demirov and Pinardi, 2007) and deep water formation processes enhancing its intrinsic variability (Waldman et al., 2017a, b). In addition, Waldman et al. (2018) studied the intrinsic variability in deep water formation processes in the northwestern Mediterranean Sea, finding that it contributes significantly to deep water formation interannual variability and is mostly generated by baroclinic instability.

We use a well-calibrated version of the Mediterranean Sea general circulation model used for short-term forecasting, and we produce an ensemble of simulations using the same atmospheric forcing but different realistic initial conditions. First, we characterize the 3-D spatial distribution and the seasonal characteristics of the internal ocean variability over the entire basin. Secondly, we quantify the relative importance of the internal variability with respect to the atmospherically forced response using the *noise-to-signal ratio*. In the current analysis, the *signal* is identified with the mean of the ensemble of simulations, whereas the *noise* or internal variability is approximated by the standard deviation of the ensemble members with respect to the mean. The questions we want to answer are how large the internal variability is and what its structure is in the Mediterranean basin and what the ratio between noise and signal is.

The rest of the paper is organized as follows. The experimental setup is described in Sect. 2, alongside the explanation of the rationale for the simulations and the statistical methods used. In Sect. 3 we show the evaluation of the quality of the ensemble experiment, and in Sect. 4 the internal variability's spatial distribution, seasonality, and dependence on depth are shown. Lastly, in Sect. 5 the stochastic variability is compared to the atmospherically forced variability, and their relative importance is assessed. Conclusions are summarized in the last section.

2 Model setup and simulations

The model used in this work is one of the operational versions of the forecasting system of the Mediterranean Sea (Clementi et al., 2019; Coppini et al., 2023) consisting of a coupled general circulation–wave model (Fig. 1) without tidal components. For the present work the wave component was disregarded. The model horizontal grid resolution is 1/24° (ca. 4 km) and has 141 unevenly spaced z^* levels. The model is forced by momentum, water, and heat fluxes computed through bulk formulae using the operational analysis and forecast fields from the European Centre for Medium-Range Weather Forecasts (ECMWF). The ECMWF atmo-

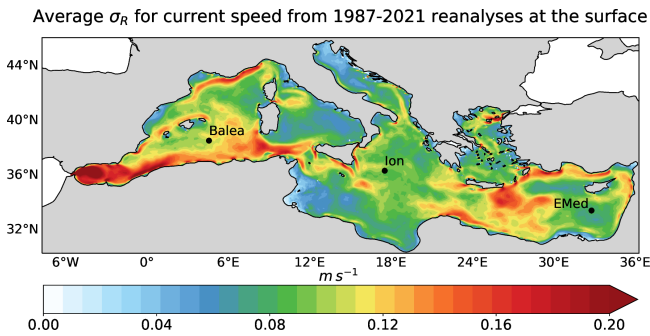


Figure 1. Average interannual spread σ_R in the Mediterranean Sea at the surface computed with the reanalyses from the period 1987–2021 (see Sect. 3). σ_R is computed as the spread of an ensemble composed of the current speed field of each year from 1987 to 2021. The dots indicate the locations that were chosen for the analysis: Balearic Islands (Balea), Ionian Sea (Ion), and eastern Mediterranean Sea (EMed).

spheric boundary conditions have a horizontal resolution of $1/8^\circ$ up to December 2020 and of $1/10^\circ$ after. This change in the forcing's horizontal resolution is irrelevant since during the analyzed period all simulations are forced by the same atmospheric fields. For more details on the specific model implementation, refer to Coppini et al. (2023).

Following the idea in Penduff et al. (2018) and in Tang et al. (2020), an ensemble of 20 simulations of the Mediterranean Sea is generated with the same atmospheric conditions but with different start dates and consequently different run times. Each simulation is initialized every 3 months starting from January 2016 to October 2020. The initial conditions are taken from the Copernicus Marine Service analyses (Clementi et al., 2019), and all simulations last up to December 2021, as explained in Fig. 2. Thus, the ensemble spread, related to internal variability, is generated by the different initial conditions. It is clear that the further back the start date of the simulation is, the longer it has been since the last analysis and internal nonlinearities started to deviate the solution from it. The same results could be obtained by just adopting different computing platforms, as proved in Lin et al. (2023a), since what is needed is just small disturbances. It is important to notice that the choice of having an ensemble of 20 members was somewhat arbitrary, even if it was the largest number of members compatible with our computational resources and returned results similar to a smaller ensemble of only 5 members (Figs. S4 and S5 in the Supplement).

In addition, each ensemble member is driven through bulk formulae by an identical atmospheric forcing function and atmospheric conditions, but variations in air–sea fluxes within the ensemble arise due to differences in oceanic variables (Bessières et al., 2017). This configuration gives realistic results but induces, for instance, an implicit relaxation of the sea surface temperature (SST) towards the same equivalent

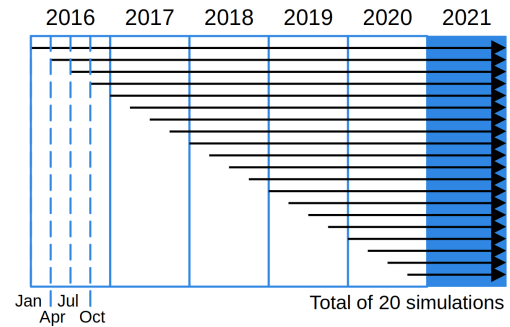


Figure 2. Scheme of the ensemble of 20 multiyear ocean simulations (black arrows). The blue box indicates the analyzed year.

air temperature, thereby damping the SST spread (Barnier et al., 1995).

The analysis is performed over the entire Mediterranean Sea at fixed depth levels (1, 20, 50, 100, 200, 500, 1000 m) and at some locations, indicated by the dots in Fig. 1, that are chosen to characterize the entire basin from the western to the eastern side. Limiting the analysis to the first 1000 m of the water column was justified in order to capture a meaningful noise-to-signal ratio (N/S). The deeper levels showed decreased spread and decreasing atmospheric influence, as expected for the large-scale circulation. Despite its arbitrariness, this boundary ensures a practical balance between vertical variability and statistical significance. Furthermore, starting from daily outputs, we focus on the seasonal timescale, in particular considering the 4-month winter and summer seasons defined in Artegiani et al. (1997) for the Mediterranean region, i.e., January–April (JFMA) and July–October (JASO), respectively.

Lastly, it is essential to acknowledge that the model we used is not everywhere eddy-resolving but mainly eddy-permitting. This is a consequence of the fact that the first Rossby radius of deformation in the Mediterranean Sea varies from 3 to 13 km (Beuvier et al., 2012) with larger values in the basin's interior and the southern areas. In contrast, in the Adriatic Sea and the Gulf of Gabes, the Rossby radius is generally smaller than the model's horizontal resolution, thus possibly artificially decreasing the importance of internal variability.

Statistical methods

We employ basic ensemble statistics to measure the internal and forced variability in the ocean. The ensemble mean of the simulations is considered to represent the forced response of all members to the common forcing, hereafter indicated with the signal. Subtracting this quantity from each member we obtain the stochastic variations, uncorrelated between the members (Penduff et al., 2018; Leroux et al., 2018). Consequently, the internal ocean variability σ_I can be computed considering the discrepancy of each member from the en-

semble average, i.e., the *ensemble standard deviation* or *ensemble spread* or *noise*, at each grid point (i, j):

$$\sigma_1(i, j, t) = \sqrt{\frac{1}{N-1} \sum_{n=1}^N [f_n(i, j, t) - f_{\text{mean}}(i, j, t)]^2}, \quad (1)$$

where $N = 20$ is the ensemble size, f_n is the n th member and f_{mean} is the ensemble mean. On the other hand, the atmospherically forced variability σ_A , that is the variability shared by all simulations, is given by the evolution of the single-member means expressed by its temporal standard deviation:

$$\sigma_A(i, j; \tau) = \sqrt{\frac{1}{\tau-1} \sum_{t=1}^{\tau} [f_{\text{mean}}(i, j, t) - \overline{f_{\text{mean}}}(i, j)]^2}, \quad (2)$$

where $\overline{f_{\text{mean}}}$ is the temporal average of the ensemble mean over the chosen period τ , i.e., 120 d corresponding to a season. In the present work, we use internal or intrinsic variability and ensemble spread interchangeably, the latter being the mathematical formulation of the former. To compare Eqs. (1) and (2), we consider the ratio, called noise-to-signal ratio, as the temporal average of the internal variability over the forced variability during the same period:

$$\frac{N}{S}(i, j; \tau) = \frac{(\sigma_1(i, j, t))_{\tau}}{\sigma_A(i, j; \tau)}. \quad (3)$$

3 Variability: model output compared to reanalysis

To evaluate the quality of the model simulations, the ensemble members are compared to the reanalysis of the year 2021 (Escudier et al., 2021) produced approximately with the same model but assimilating drifting profiles, satellite sea surface temperature, and altimetry.

For current velocities, we compared the internal variability found in the simulations and the standard deviation computed from the 2021 reanalysis, hereafter called σ_{2021} . We would like to verify that σ_1 is not overestimated when compared to the natural variability represented by the standard deviation of the reanalysis. We found that the ensemble members' internal variability is generally smaller than both the interannual variability σ_R computed from the 1987–2021 reanalyses (Fig. 1) and the standard deviation σ_{2021} of the 2021 reanalysis (Fig. 3), with the only exception of the region around the Balearic Islands. We argue that the ensemble internal variability is comparable with the natural variability in the Mediterranean Sea at all depths and seasons.

Another evaluation of the ensemble spread is done by comparing it to the RMSE of the ensemble mean with respect to the 2021 reanalysis r , as suggested in Fortin et al. (2014):

$$\sqrt{\sigma^2} = \sqrt{\frac{N}{N+1}} \text{RMSE}, \quad (4)$$

where $\sqrt{\sigma^2} = \sqrt{\frac{1}{\tau} \sum_{t=1}^{\tau} \text{var}(t)}$ and $\text{RMSE} = \sqrt{\frac{1}{\tau} \sum_{t=1}^{\tau} (f_{\text{mean}}(t) - r(t))^2}$, with $\tau \rightarrow \infty$ since this relation holds for large values of τ , and this is the reason we considered $\tau = 365$ d corresponding to the entire 2021.

It is important to note that both Eqs. (4) and (1) depend on the ensemble size N . Figure 4 and Fig. S1 show the values of the mean ensemble variance versus the RMSE for temperature and current speed, respectively, for each grid point averaged over the entire year and at different depths. Points above the line described by Eq. (4) characterize an overdispersive ensemble, whereas those below show an underdispersive ensemble. Overall, the present ensemble can be considered underdispersive. For temperature, the ensemble variance and the uncertainty peak at roughly 30 m depth (Fig. 4), and in the case of current speed, both the ensemble variance and the RMSE decrease with depth (Fig. S1).

Lastly, the ensemble spread and the noise-to-signal ratio were computed also for the year 2020 (see Figs. S16–S19) but with only 16 simulations, resulting in the same findings as for 2021, proving that these are not peculiar to the chosen year.

4 Characterization of internal variability

The ensemble spread for the current speed v and potential temperature T is shown in Fig. 5 at 30 m depth for both seasons (see Figs. S6–S7 for all depth levels).

In the literature, Hecht et al. (1988) have described the eastern Levantine thermocline's seasonal variations, showing it to be located between 20 and 40 m depth. Thus, we refer to 30 m as the average depth of the seasonal thermocline.

It is evident that internal variability for currents is high amplitude at the surface and that in both seasons its spatial pattern is unchanged with depth while decreasing in intensity. In winter, the areas with the highest intrinsic variability (0.12 – 0.15 m s^{-1}) are distributed along the southern parts of the basin, while in summer, an equally significant presence of internal variability is found in localized areas: in the Ionian Sea and in the westernmost part of the basin. In both seasons, the Adriatic Sea and the Gulf of Gabes show the minimum values of the ensemble spread (less than 0.03 m s^{-1}).

For temperature, the ensemble spread exhibits a much more pronounced seasonality. In winter, the maximum values are of the order of $0.5 \text{ }^\circ\text{C}$ and are mainly located in the eastern Mediterranean. Moreover, the spatial distribution of the spread remains practically constant along the water column up to a depth of 100 m. During summer the ensemble spread is largest at depths between 20 and 30 m (about $1.5 \text{ }^\circ\text{C}$), which coincides with the seasonal upper-thermocline center depth. The spread is again low in the Adriatic Sea and the Gulf of Gabes extended shelf areas. In fact, over shelf areas, the external forcing or signal exerts a more significant influence with respect to deep ocean areas (Tang et al.,

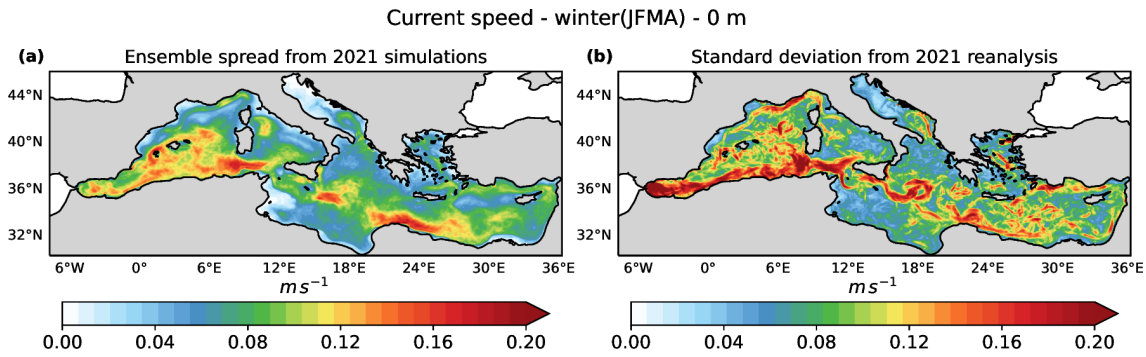


Figure 3. Comparison between the winter-averaged ensemble spread σ_I with $N = 20$ (a) relative to current speed computed from the ensemble of simulations and the corresponding seasonal standard deviation σ_{2021} (b) obtained from the 2021 reanalysis.

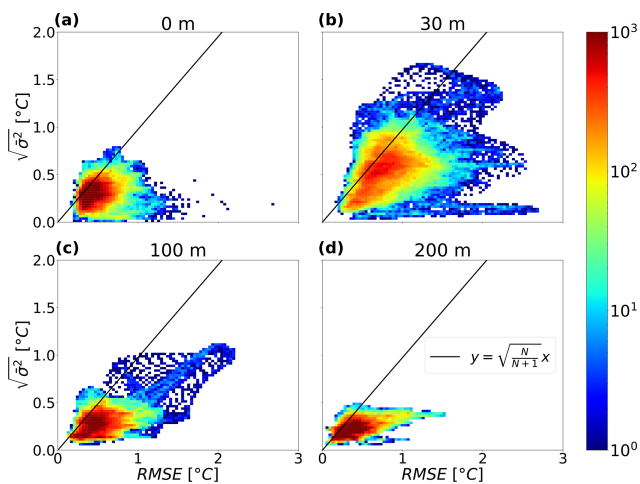


Figure 4. Ensemble dispersion relative to sea potential temperature: verification of Eq. (4) averaged over the entire year 2021 for each grid point at the surface (a), at 30 m (b), at 100 m (c), and at 200 m (d). The black line indicates the ideal relation expressed in Eq. (4).

2020; Lin et al., 2022). For depths greater than 100–200 m, the seasonal trend disappears for both current and temperature spread (see Fig. S8).

The vertical profile of the ensemble spread follows the vertical temperature gradient, as shown in Fig. 6. It peaks at the seasonal thermocline center depth, i.e., at the depth of the vertical temperature gradient maximum. In other words, the ensemble spread is greater where strong temperature gradients are present since small differences among the simulations are amplified by the significant changes in the temperature field at these depths. However, the relation between ensemble spread and vertical temperature gradient varies depending on the location: in the Ionian Sea (Ion in Fig. 6) and in the Balearic Islands (Balea), the alignment between the two curves is notably robust. Conversely, in the eastern Mediterranean (EMed), the peak of the temperature gradient occurs at approximately 20 m, whereas the maximum of

σ_I is found at 40 m. We argue that, during summer, thermocline processes exhibit significant internal variability and that the spread observed at the peak of the vertical temperature gradient may arise from various mechanisms. First, baroclinic instability localized there can generate internal variability. Secondly, changes in the position and strength of eddies can cause upwelling or downwelling, thereby influencing the mixed layer depth and consequently the mid-depth of the thermocline (Figs. S10 and S11).

5 Comparison between noise and signal

In order to quantify the relative importance of the internal variability with respect to the atmospherically forced response, the noise-to-signal ratio (Eq. 3) is computed. Figure 7 summarizes the basin-averaged vertical profile of N/S across the two seasons at the discrete depth levels defined in Sect. 2. The N/S for T is smaller than 1 up to 100 m (about 0.3 at the surface), and it increases with depth. In the surface layers, it shows greater values in winter, whereas at greater depths it attains systematically larger values (approximately equal to 6) in summer. On the other hand, the current speed's N/S is always greater than 1: it rises steadily in the first 50 m, reaching a maximum at 200 m in summer and winter, and then slightly decreases with depth. Thus, even though σ_I has its maximum at some intermediate depth for T and it is maximum at the surface for v , the N/S is greater at depth due to the diminishing importance of the atmospheric forcing with increasing depth. Moreover, whereas for v the internal variability is always dominant, for T the atmospheric response has a dominant influence in the surface layers, especially in winter.

As regards the spatial distribution of the noise-to-signal ratio, as expected the Adriatic Sea and the Gulf of Gabes are the regions with the smallest values of N/S for both T and v . For potential temperature (see Fig. 8) N/S in summer is less than 1 over the entire Mediterranean Sea at the surface, but it increases with depth, especially along the African coast in the western Mediterranean and in the northern part of the

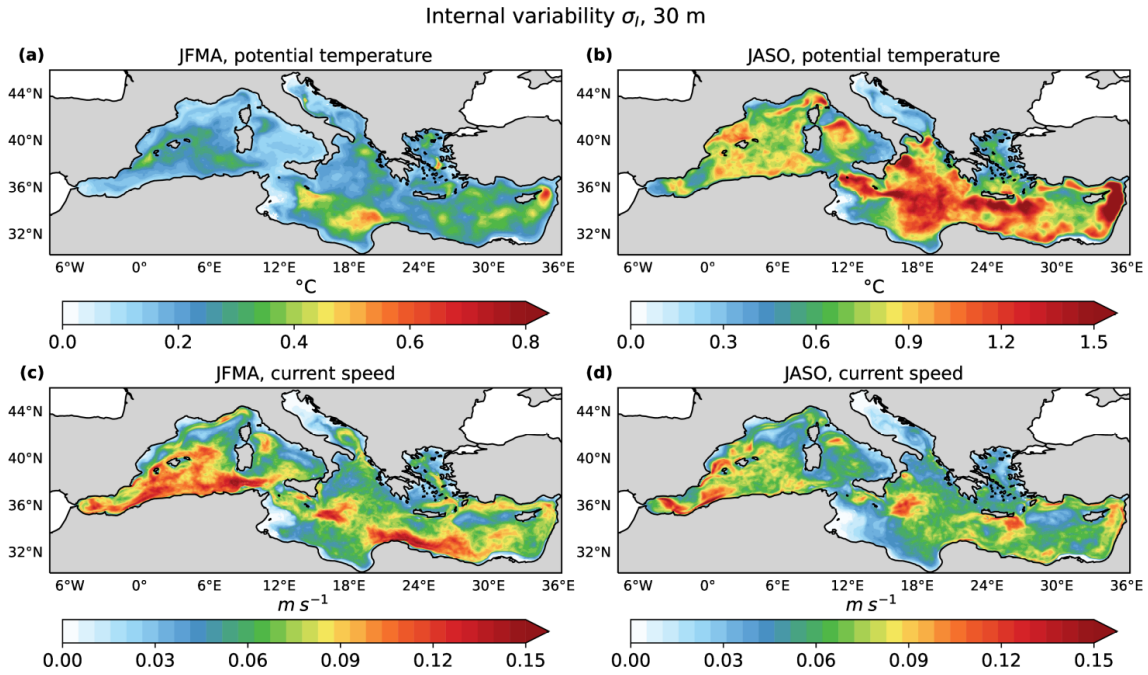


Figure 5. Seasonally averaged ensemble spread at 30 m depth for seawater potential temperature both in winter (a) and in summer (b). Similarly for current speed in (c) and (d).

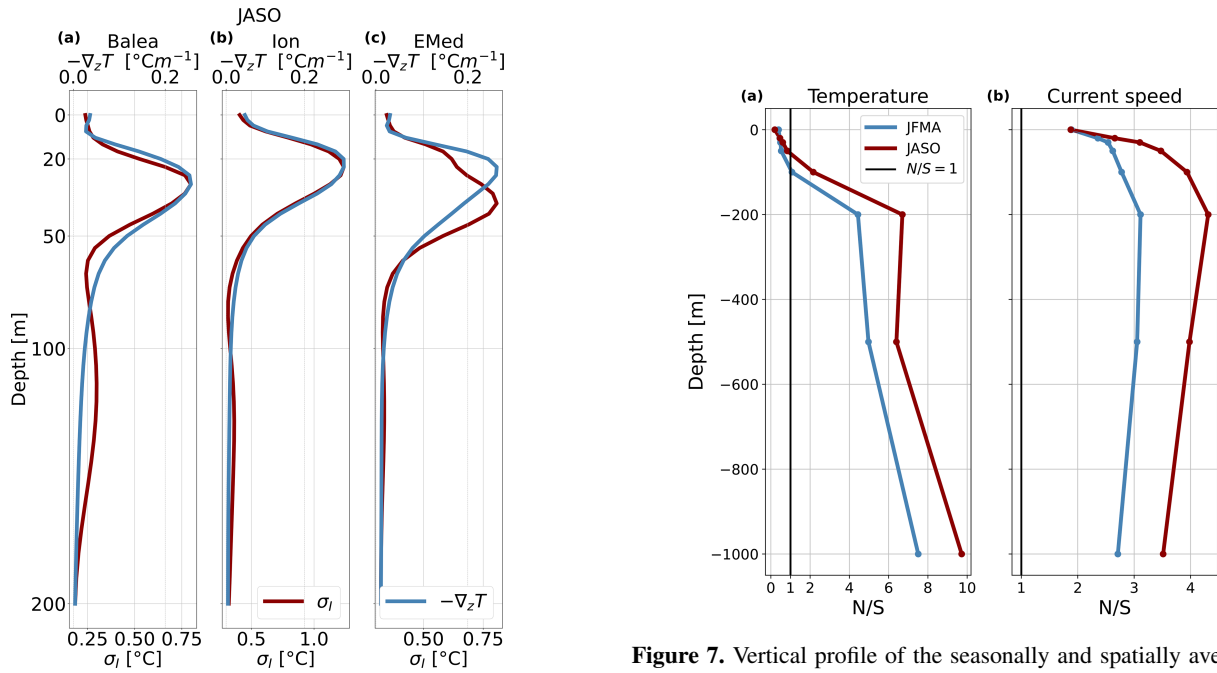


Figure 6. Seasonally averaged vertical profile of the ensemble spread σ_I (red) for potential temperature and of the vertical temperature gradient $-\nabla T_z$ (blue) in summer at the Balearic Islands (Balea) (a), Ionian Sea (Ion) (b), and eastern Mediterranean Sea (EMed) (c).

Figure 7. Vertical profile of the seasonally and spatially averaged noise-to-signal ratio for potential temperature (a) and current speed (b). Red represents summer, whereas blue is winter, and the vertical black lines correspond to $N/S = 1$.

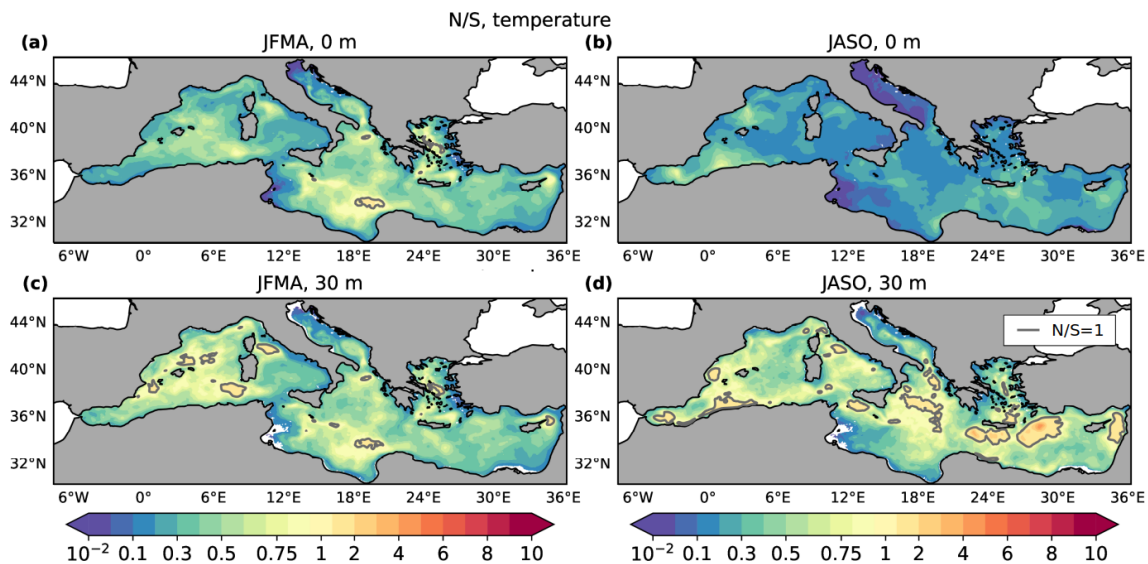


Figure 8. Seasonally averaged N/S for seawater potential temperature in winter both at the surface (a) and at 30 m depth (c). Analogously for summer in (b) and (d). The gray lines represent the isolines at $N/S = 1$.

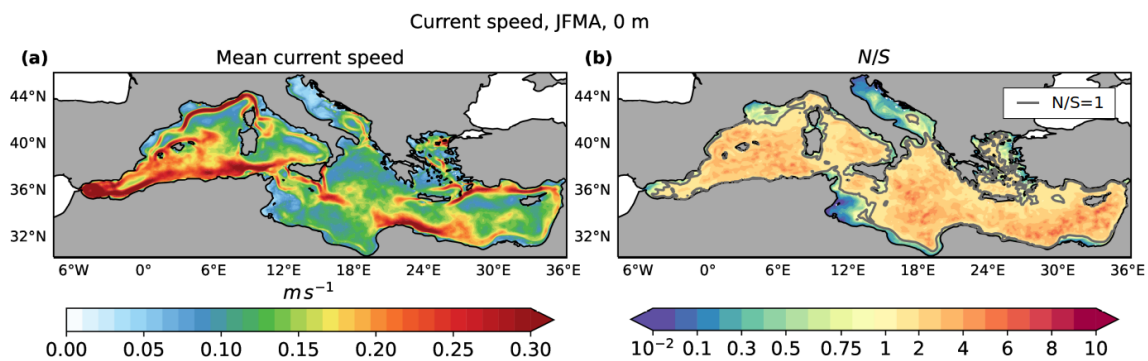


Figure 9. Seasonal average (winter, JFMA) at the surface of the ensemble mean (a) and of the N/S (b) for the speed of the current. The gray lines in the right plot represent the isolines at $N/S = 1$.

eastern Mediterranean. In winter, instead, in the Ionian Sea, north of the Gulf of Sidra, N/S is greater than unity, and it tends to grow with depth mainly in this region and along the coast of Spain in the western Mediterranean. Conversely, the model-resolved mesoscale activity contributes to σ_1 for v in vast open-ocean areas of the basin. Figure 9 shows that N/S is higher than 1 in large open-ocean areas offshore from vigorous northern and southern boundary currents (northern Liguro-Provencal current, the Algerian current, the Asia Minor current, etc.). We argue that this internal variability is due to mesoscales. Some of the intense current regions, such as the Gibraltar inflow current and part of the Liguro-Provencal current, show a relevant contribution from external forcings, the Atlantic water inflow for the former and the wind stress curl for the latter, as documented by many authors (Herbaut et al., 1997; Molcard et al., 2002). In the shallow areas of the Adriatic and Gulf of Gabes, where the external forcing is dominant, the mean flow probably fluctuates with the forc-

ings and prevents the onset of instabilities and the production of internal variability.

6 Discussion and conclusions

In the present work, we used a simulation ensemble approach to study, for the first time in the Mediterranean Sea, the internal variability or noise versus the atmospherically forced signal. Producing an ensemble of 20 simulations of the Mediterranean Sea in 2021 with different start dates but forced by the same atmospheric conditions, we were able to characterize the internal ocean variability σ_1 as opposed to the forced response of the ocean. Moreover, we used the noise-to-signal ratio N/S to measure the relative importance of the former compared to the latter. We characterized and quantified the internal variability and N/S as regards their vertical profiles, seasonal cycle, and spatial patterns for temperature and cur-

rent speed. In general, the atmospherically forced response tends to decrease with depth and thrives instead in the extended shelf areas of the basin such as the Adriatic Sea and the Gulf of Gabes. Relative to temperature, the atmospheric forcing is dominant in the first 50 m of the water column in summer and in the first 100 m in winter. Furthermore, internal variability is dominant in most of the open-ocean regions of the Mediterranean Sea due to the intense mesoscale variability offshore from intense northern and southern mean current systems. To note, some of the most intense currents have components that are externally forced, such as the Alboran current and segments of the Liguro-Provençal current system. Lastly, the intrinsic variability shows a large seasonal cycle in temperature with a sharp maximum in summer at roughly 30 m depth and a much less pronounced one at about 100 m depth in winter. The vertical profile of the spread in summer is probably related to the large variability in the upper thermocline due to internal variability. Regarding current speed, the internal variability is dominant at all depths and largest at the surface.

The assessment of the internal oceanic variability is crucial for tackling the issue of estimating the ocean's intrinsic predictability and comprehending the distinct roles of internal instabilities and external forcings in shaping ocean dynamics. Furthermore, this research serves as an additional validation of the efficient yet straightforward nature of this ensemble statistic, derived from the theory of stochastic climate models, whose aim is not to investigate specific hydrodynamic processes but to study the system's properties and statistics (Lin et al., 2023b). Moreover, the noise-to-signal ratio proves to be an effective diagnostic indicator. Last but not least, the production of internal variability itself has been assessed, further proving the main idea behind stochastic climate model theory: in a dynamical system featuring the coexistence of diverse temporal scales and the possibility to distinguish between transient and mean components, variations can arise from their internal interactions without implying any external factor.

A limitation of our study is the underestimation of the internal variability stemming from the model's horizontal resolution of $1/24^\circ$ which results in its being too coarse for resolving mesoscale eddies everywhere in the Mediterranean Sea. Such an underestimation could be particularly significant in the Adriatic Sea and the Gulf of Gabes where the spatial scales of mesoscale eddies tend to be smaller than the model's horizontal resolution. Thus, this could be an additional factor causing the small values of the ensemble spread in these regions. Nonetheless, the present study shows the importance of internal processes as opposed to the atmospheric influence compatible with the model resolution.

An extension of this analysis could involve the incorporation of tides into the general circulation model especially because tides have an important effect on the whole Mediterranean Sea (McDonagh et al., 2023), including the Strait of Gibraltar (Gonzalez et al., 2021), which could in turn result

in differences in the generation and characterization of internal variability. For instance, the recent works by Lin et al. (2022, 2023c) on the internal variability in the Bohai and Yellow Sea show that tidal forcing inhibits the generation of internal variability at large scales and that baroclinic instability might significantly drive the latter. Moreover, they suggest that the memory of the system is a critical factor in the generation of internal variability at large scales: the spectrum of the intrinsic variability with tides is less *red* than the one without. Since in a first-order autoregressive process, as the mathematical formulation of stochastic climate models, the *redness* of the spectrum is a measure of the memory of the system, i.e., a measure of how long an anomaly will last once formed, this comparison shows that tides and winter conditions tend to decrease the system's memory, inhibiting anomalies from persisting and upscaling. The study of the importance of tides in the generation of internal variability would be interesting to be redone in a deep basin such as the Mediterranean Sea. Lastly, given the importance of submesoscales in several regions of the Mediterranean Sea (Trotta et al., 2017; CALYPSO, CAL, 2024; Solodoch et al., 2023) future work could include the addition of submesoscale variability as a source of ocean internal variability.

Data availability. Results from these simulations are freely available at <https://doi.org/10.5281/zenodo.10371026> (Benincasa et al., 2024).

Supplement. The supplement related to this article is available online at: <https://doi.org/10.5194/os-20-1003-2024-supplement>.

Author contributions. All authors contributed to the design of this work. HvS, GL, and NP formulated the initial problem idea; RB carried out all simulations and analyzed the output; and under the guidance of GL, RB developed the analysis tools. All authors contributed to the interpretation of the results

Competing interests. The contact author has declared that none of the authors has any competing interests.

Disclaimer. Publisher's note: Copernicus Publications remains neutral with regard to jurisdictional claims made in the text, published maps, institutional affiliations, or any other geographical representation in this paper. While Copernicus Publications makes every effort to include appropriate place names, the final responsibility lies with the authors.

Acknowledgements. Roberta Benincasa thanks Giovanni Liguori, Nadia Pinardi, and Hans von Storch for their guidance and mentorship throughout this work. The research presented in this paper

was carried out on the supercomputer facilities of CMCC in Lecce (Italy).

Financial support. Support for Nadia Pinardi and Giovanni Liguori work came from the EU H2020 EuroSea Project.

Review statement. This paper was edited by Anne Marie Treguier and reviewed by two anonymous referees.

References

- Arbic, B. K., Müller, M., Richman, J. G., Shriver, J. F., Morten, A. J., Scott, R. B., Sérazin, G., and Penduff, T.: Geostrophic turbulence in the frequency–wavenumber domain: Eddy-driven low-frequency variability, *J. Phys. Oceanogr.*, 44, 2050–2069, 2014.
- Artegiani, A., Paschini, E., Russo, A., Bregant, D., Raicich, F., and Pinardi, N.: The Adriatic Sea general circulation. Part I: Air–sea interactions and water mass structure, *J. Phys. Oceanogr.*, 27, 1492–1514, 1997.
- Barnier, B., Siefridt, L., and Marchesiello, P.: Thermal forcing for a global ocean circulation model using a three-year climatology of ECMWF analyses, *J. Marine Syst.*, 6, 363–380, 1995.
- Benincasa, R., Liguori, G., Pinardi, N., and von Storch, H.: Simulations used in the Ocean Science Journal submission titled “Internal and forced ocean variability in the Mediterranean Sea” by Benincasa et al., 2024, Zenodo [data set], <https://doi.org/10.5281/zenodo.10371026>, 2024.
- Beuvier, J., Béranger, K., Lebeau-pin Brossier, C., Somot, S., Sevault, F., Drillet, Y., Bourdallé-Badie, R., Ferry, N., and Lyard, F.: Spreading of the Western Mediterranean Deep Water after winter 2005: Time scales and deep cyclone transport, *J. Geophys. Res.-Oceans*, 117, C07022, <https://doi.org/10.1029/2011JC007679>, 2012.
- Bessières, L., Leroux, S., Brankart, J.-M., Molines, J.-M., Moine, M.-P., Bouttier, P.-A., Penduff, T., Terray, L., Barnier, B., and Sérazin, G.: Development of a probabilistic ocean modelling system based on NEMO 3.5: application at eddying resolution, *Geosci. Model Dev.*, 10, 1091–1106, <https://doi.org/10.5194/gmd-10-1091-2017>, 2017.
- Bonaduce, A., Cipollone, A., Johannessen, J. A., Staneva, J., Raj, R. P., and Aydogdu, A.: Ocean mesoscale variability: A case study on the Mediterranean Sea from a re-analysis perspective, *Front. Earth Sci.*, 9, 724879, <https://doi.org/10.3389/feart.2021.724879>, 2021.
- CAL: Coherent Lagrangian Pathways from Surface Ocean to Interior, <https://calypsodri.whoi.edu/>, last access: 5 April 2024.
- Clementi, E., Pistoia, J., Escudier, R., Delrosso, D., Drudi, M., Grandi, A., Lecci, R., Cretì, S., Ciliberti, S., Coppini, G., Masina, S., and Pinardi, N.: Mediterranean Sea Analysis and Forecast (CMEMS MED-Currents, EAS5 system) (Version 1), Copernicus Monitoring Environment Marine Service (CMEMS) [data set], https://doi.org/10.25423/CMCC/MEDSEA_ANALYSIS_FORECAST_PHY_006_013_EAS5, 2019.
- Coppini, G., Clementi, E., Cossarini, G., Salon, S., Korres, G., Ravidas, M., Lecci, R., Pistoia, J., Goglio, A. C., Drudi, M., Grandi, A., Aydogdu, A., Escudier, R., Cipollone, A., Lyubartsev, V., Mariani, A., Cretì, S., Palermo, F., Scuro, M., Masina, S., Pinardi, N., Navarra, A., Delrosso, D., Teruzzi, A., Di Biagio, V., Bolzon, G., Feudale, L., Coidezza, G., Amadio, C., Brosich, A., Miró, A., Alvarez, E., Lazzari, P., Solidoro, C., Oikonomou, C., and Zacharioudaki, A.: The Mediterranean Forecasting System – Part 1: Evolution and performance, *Ocean Sci.*, 19, 1483–1516, <https://doi.org/10.5194/os-19-1483-2023>, 2023.
- Demirov, E. K. and Pinardi, N.: On the relationship between the water mass pathways and eddy variability in the Western Mediterranean Sea, *J. Geophys. Res.-Oceans*, 112, C02024, <https://doi.org/10.1029/2005JC003174>, 2007.
- Escudier, R., Clementi, E., Cipollone, A., Pistoia, J., Drudi, M., Grandi, A., Lyubartsev, V., Lecci, R., Aydogdu, A., Delrosso, D., Omar, M., Masina, S., Coppini, G., and Pinardi, N.: A high resolution reanalysis for the Mediterranean Sea, *Front. Earth Sci.*, 9, 702285, <https://doi.org/10.3389/feart.2021.702285>, 2021.
- Fortin, V., Abaza, M., Anctil, F., and Turcotte, R.: Why should ensemble spread match the RMSE of the ensemble mean?, *J. Hydrometeorol.*, 15, 1708–1713, 2014.
- Gonzalez, N., Waldman, R., Sannino, G., Giordani, H., and Somot, S.: A new perspective on tidal mixing at the Strait of Gibraltar from a very high-resolution model of the Mediterranean Sea, EGU General Assembly 2021, online, 19–30 Apr 2021, EGU21-3971, <https://doi.org/10.5194/egusphere-egu21-3971>, 2021.
- Harrison, D. and Robinson, A.: Energy analysis of open regions of turbulent flows – Mean eddy energetics of a numerical ocean circulation experiment, *Dynam. Atmos. Oceans*, 2, 185–211, 1978.
- Hasselmann, K.: Stochastic climate models part I. Theory, *Tellus*, 28, 473–485, 1976.
- Hecht, A., Pinardi, N., and Robinson, A. R.: Currents, water masses, eddies and jets in the Mediterranean Levantine Basin, *J. Phys. Oceanogr.*, 18, 1320–1353, 1988.
- Herbaut, C., Martel, F., and Crépon, M.: A sensitivity study of the general circulation of the Western Mediterranean Sea. Part II: the response to atmospheric forcing, *J. Phys. Oceanogr.*, 27, 2126–2145, 1997.
- Hogan, E. and Sriv, R.: The effect of internal variability on ocean temperature adjustment in a low-resolution CESM initial condition ensemble, *J. Geophys. Res.-Oceans*, 124, 1063–1073, 2019.
- Jochum, M. and Murtugudde, R.: Internal variability of the tropical Pacific Ocean, *Geophys. Res. Lett.*, 31, L14309, <https://doi.org/10.1029/2004GL020488>, 2004.
- Jochum, M. and Murtugudde, R.: Internal variability of Indian ocean SST, *J. Climate*, 18, 3726–3738, 2005.
- Leroux, S., Penduff, T., Bessières, L., Molines, J.-M., Brankart, J.-M., Sérazin, G., Barnier, B., and Terray, L.: Intrinsic and atmospherically forced variability of the AMOC: Insights from a large-ensemble ocean hindcast, *J. Climate*, 31, 1183–1203, 2018.
- Le Traon, P. Y., Reppucci, A., Alvarez Fanjul, E., et al.: From observation to information and users: The Copernicus Marine Service perspective, *Front. Mar. Sci.*, 6, 234, <https://doi.org/10.3389/fmars.2019.00234>, 2019.
- Lin, L., von Storch, H., Guo, D., Tang, S., Zheng, P., and Chen, X.: The effect of tides on internal variability in the Bohai and Yellow Sea, *Dynam. Atmos. Oceans*, 98, 101301, <https://doi.org/10.1016/j.dynatmoce.2022.101301>, 2022.
- Lin, L., von Storch, H., and Chen, X.: Seeding Noise in Ensembles of Marginal Sea Simulations – The Case of Bohai and Yel-

- low Sea, *Advances in Computer and Communication*, 4, 70–73, 2023a.
- Lin, L., von Storch, H., and Chen, X.: The Stochastic Climate Model helps reveal the role of memory in internal variability in the Bohai and Yellow Sea, *Communications Earth & Environment*, 4, 347, <https://doi.org/10.1038/s43247-023-01018-7>, 2023b.
- Lin, L., von Storch, H., Chen, X., Jiang, W., and Tang, S.: Link between the internal variability and the baroclinic instability in the Bohai and Yellow Sea, *Ocean Dynam.*, 73, 793–806, 2023c.
- Lorenz, E. N.: Climate predictability, in: *The physical basis of climate and climate modelling* (WMO GARP Publ. Ser. no. 16), 132–136, Geneva, World Meteorological Organization, 1975.
- McDonagh, B., Clementi, E., and Pinardi, N.: The characteristics and effects of tides on the general circulation of the Mediterranean Sea, EGU General Assembly 2023, Vienna, Austria, 24–28 Apr 2023, EGU23-14117, <https://doi.org/10.5194/egusphere-egu23-14117>, 2023.
- McWilliams, J. C.: Modeling the oceanic general circulation, *Annu. Rev. Fluid Mech.*, 28, 215–248, 1996.
- Molcard, A., Pinardi, N., Iskandarani, M., and Haidvogel, D.: Wind driven general circulation of the Mediterranean Sea simulated with a Spectral Element Ocean Model, *Dynam. Atmos. Oceans*, 35, 97–130, 2002.
- Penduff, T., Sérazin, G., Leroux, S., Close, S., Molines, J.-M., Barnier, B., Bessières, L., Terray, L., and Maze, G.: Chaotic variability of ocean heat content: climate-relevant features and observational implications, *Oceanography*, 31, 63–71, 2018.
- Pinardi, N., Zavatarelli, M., Adani, M., Coppini, G., Fratianni, C., Oddo, P., Simoncelli, S., Tonani, M., Lyubartsev, V., Dobricic, S., and Bonaduce, A.: Mediterranean Sea large-scale low-frequency ocean variability and water mass formation rates from 1987 to 2007: A retrospective analysis, *Prog. Oceanogr.*, 132, 318–332, 2015.
- Pinardi, N., Cessi, P., Borile, F., and Wolfe, C. L.: The Mediterranean sea overturning circulation, *J. Phys. Oceanogr.*, 49, 1699–1721, 2019.
- Robinson, A. R., Leslie, W. G., Theoharis, A., and Lascaratos, A.: Mediterranean sea circulation, *Ocean currents*, 2001, 1689–1705, <https://doi.org/10.1006/rwos.2001.0376>, 2001.
- Sérazin, G., Penduff, T., Grégorio, S., Barnier, B., Molines, J.-M., and Terray, L.: Intrinsic variability of sea level from global ocean simulations: Spatiotemporal scales, *J. Climate*, 28, 4279–4292, 2015.
- Soldatenko, S. and Yusupov, R.: Predictability in Deterministic Dynamical Systems with Application to Weather Forecasting and Climate Modelling, in: *Dynamical Systems-Analytical and Computational Techniques*, edited by: Reyhanoglu, M., p. 101, IntechOpen, <https://doi.org/10.5772/66752>, 2017.
- Solodoch, A., Barkan, R., Verma, V., Gildor, H., Toledo, Y., Khain, P., and Levi, Y.: Basin-Scale to Submesoscale Variability of the East Mediterranean Sea Upper Circulation, *J. Phys. Oceanogr.*, 53, 2137–2158, 2023.
- Tang, S., von Storch, H., Chen, X., and Zhang, M.: “Noise” in climatologically driven ocean models with different grid resolution, *Oceanologia*, 61, 300–307, 2019.
- Tang, S., von Storch, H., and Chen, X.: Atmospherically forced regional ocean simulations of the South China Sea: scale dependency of the signal-to-noise ratio, *J. Phys. Oceanogr.*, 50, 133–144, 2020.
- Trotta, F., Pinardi, N., Fenu, E., Grandi, A., and Lyubartsev, V.: Multi-nest high-resolution model of submesoscale circulation features in the Gulf of Taranto, *Ocean Dynam.*, 67, 1609–1625, 2017.
- von Storch, H., von Storch, J.-S., and Müller, P.: Noise in the climate system—ubiquitous, constitutive and concealing, *Mathematics Unlimited – 2001 and Beyond*, Springer, Berlin, Heidelberg, 1179–1194, https://doi.org/10.1007/978-3-642-56478-9_62, 2001.
- Waldman, R., Herrmann, M., Somot, S., Arsouze, T., Benshila, R., Bosse, A., Chanut, J., Giordani, H., Sevault, F., and Testor, P.: Impact of the mesoscale dynamics on ocean deep convection: The 2012–2013 case study in the northwestern Mediterranean sea, *J. Geophys. Res.-Oceans*, 122, 8813–8840, 2017a.
- Waldman, R., Somot, S., Herrmann, M., Bosse, A., Caniaux, G., Estournel, C., Houpert, L., Prieur, L., Sevault, F., and Testor, P.: Modeling the intense 2012–2013 dense water formation event in the northwestern Mediterranean Sea: Evaluation with an ensemble simulation approach, *J. Geophys. Res.-Oceans*, 122, 1297–1324, 2017b.
- Waldman, R., Somot, S., Herrmann, M., Sevault, F., and Isachsen, P. E.: On the chaotic variability of deep convection in the Mediterranean Sea, *Geophys. Res. Lett.*, 45, 2433–2443, 2018.